AIP | Journal of Applied Physics

Evidence of improved ferroelectric phase stabilization in Nd and Sc co-substituted BiFeO3

T. Durga Rao1 and Saket Asthana1,a)
1 Advanced Functional Materials Laboratory, Department of Physics, Indian Institute of Technology Hyderabad, Andhra Pradesh–502205, India

AIP | Journal of Applied Physics 116, 164102 (2014).

http://dx.doi.org/10.1063/1.4898805

Evidence of improved ferroelectric phase stabilization in Nd and Sc co-substituted $BiFeO_3$

T Durga Rao, Saket Asthana*

Advanced Functional Materials Laboratory, Department of Physics,
Indian Institute of Technology Hyderabad, Telangana– 502205, India
** Author for Correspondence: asthanas@iith.ac.in*

Abstract

Polycrystalline $BiFeO_3$ and $Bi_{0.9}Nd_{0.1}Fe_{1-x}Sc_xO_3$ (x = 0, 0.05 and 0.10) multiferroic compounds were prepared using conventional solid-state route. X-ray diffraction studies and Raman measurements indicated that the compounds were crystallized in rhombohedral structure with *R3c* space group. Weak ferromagnetism was induced due to the suppression of canted spin structure in the substituted compounds. Both remnant magnetization (M_r) and coercive field (H_c) were enhanced in Nd and Sc substituted compounds. Further, Néel temperature T_N was decreased from 644 K for $BiFeO_3$ to 550 K for $Bi_{0.9}Nd_{0.1}Fe_{0.9}Sc_{0.1}O_3$ compound due to weakening of magnetic exchange interactions between *B*-site cations in the

substituted compounds. Enhanced and nearly well saturated electrical polarizations were observed in Sc substituted compounds which is attributed to the strengthening of covalent hybridization between Bi and O ions and reduction in oxygen vacancies. The remnant polarization was enhanced to 12.5 μC/cm^2 in $Bi_{0.9}Nd_{0.1}Fe_{0.9}Sc_{0.1}O_3$ compound. Impedance studies reveal that insulating character of substituted compounds is enhanced and electrical relaxations are of non-Debye type.

Key words: Multiferroics, Sc-substitution, Ferroelectric ordering, Impedance, Activation energy

Introduction

Multiferroics are the materials which simultaneously exhibit ferroelectric and (anti) ferromagnetic orders in the same phase. These materials have attracted considerable research attention because of interesting physics involved and technological applications such as spintronics, data storage devices, sensors, etc.[1,2] In multiferroics, electric polarization can be switched with the application of magnetic field and vice versa due to the existence of coupling between the ferroic orders. Among all the perovskite type single phase multiferroics, $BiFeO_3$ (BFO) is fascinating and well-studied due to its excellent ferroelectric properties at room temperature. Bulk BFO crystallizes in rhombohedral crystal structure with *R3c* space group. BFO shows *G*-type antiferromagnetic ordering below T_N = 643 K and ferroelectricity below T_C = 1103 K.[3] Ferroelectricity is resulted due to the hybridization of stereochemically active Bi 6s^2 lone pair electrons with the empty 6p^0 orbital of Bi^{3+} ion and 2p^6 orbital of O^{2-} ions. Theoretical calculations envisaged that the displacements of cations lead to the large spontaneous polarization.[4] Due to active lone pair electrons, Bi ions show relatively larger displacements compared to Fe ions. On the other hand, spin moments of Fe^{3+} ions are arranged in *G*-type antiferromagnetic order superimposed with a long range space modulated spiral spin structure (SMSS) of incommensurate wave length of 620 Å. The presence of long range SMSS inhibits the observation of linear magnetoelectric effect. And also the combination of superexchange interaction between the half-filled orbital of Fe^{3+} ions and spin-orbit coupling leads to antisymmetric Dzyaloshinskii-Moriya (DM) exchange interactions which in turn produce a weak ferromagnetic moment (~0.02 μ_B/Fe).[5,6] However, the potential of BFO in device applications is greatly hindered mainly due to the presence of leakage currents, formation of secondary phases such as $Bi_2Fe_4O_9$, $Bi_{25}FeO_{40}$ and long range spiral spin arrangement.[7] Persistent attempts have been made to minimize leakage currents and secondary phases and to induce weak ferromagnetism in BFO. Substitution of lanthanides or alkaline earth elements (La, Nd, Gd, Ca, Ba etc.) at *A*-site[8-11] and transition metal elements (Mn, Ti, Cr, etc.) at *B*-site[12,13] can effectively tune the multiferroic properties of BFO. As *A*-site and *B*-site

are mainly responsible for ferroelectric and magnetic properties respectively, it is a scientific approach to tune the multiferroic properties by simultaneous substitution of elements at the both sites. Recently, enhanced magnetization, reduced leakage current and improved dielectric properties were observed in Y and Zr,[7] La and Ti,[14] Ho and Ni,[15] Gd and Ti,[16] and Ca and Ti[17] co-substituted BFO compounds.

In this paper, Nd and Sc have been chosen to substitute at *A*-site and *B*-site respectively. Nd and Sc are chosen because; (i) the valence state of $Nd^{3+}$and Sc^{3+} ions are more stable. Substitution of these ions minimizes the Fe^{2+} ions and improves insulating character which is essential for the potential applications. (ii) substitution of Sc^{3+} for Fe^{3+} suppresses the space modulated spin structure and changes Fe-O-Fe bond angles and Fe-O bond distances which in turn improves the physical properties of BFO and (iii) as the bond enthalpies of Nd-O (703+13 kJ/mol) and Sc-O (681.6±11.3 kJ/mol) bonds are respectively stronger than that of Bi-O (337±12.6 kJ/mol) and Fe – O (390.4±17.2 kJ/mol) bond enthalpies,[18] substitution of Nd and Sc for Bi and Fe would recover the oxygen vacancies caused by volatilization of Bi atoms which in turn improves electrical insulating character by minimizing Fe^{2+} and oxygen vacancies. In the present work, structural, magnetic and electrical properties of Nd and Sc co-substituted compounds have been investigated.

Experimental details

Polycrystalline $BiFeO_3$ (BFO), $Bi_{0.9}Nd_{0.1}FeO_3$ (BNFO) and $Bi_{0.9}Nd_{0.1}Fe_{1-x}Sc_xO_3$ (BNFSO) [x = 0.05 (BNFSO5) and 0.10 (BNFSO10)] compounds were synthesized by conventional solid-state route. The detailed experimental procedure could be found elsewhere.[19] Phase analysis of the compounds was confirmed by using X-ray diffractometer (Panalytical X'pert Pro) with Cu-Kα radiation (λ = 1.5406 Å) over the angular range $20° \leq 2\theta \leq 90°$. Microstructural characterization and energy dispersive X-ray analysis (EDX) were carried out using field emission scanning electron microscope (FE-SEM, Carl Zeiss, Supra 40). Raman scattering measurements were performed on sintered and polished pellets using a laser micro Raman spectrometer (Bruker, Senterra) with an excitation laser source of 785 nm wave length. The magnetic properties were measured using PPMS with VSM assembly (Dynacool, Quantum Design, USA). Room temperature polarization (*P*) -electric field (*E*) loop measurements were carried out using aixACCT TF 2000 analyzer. The Impedance measurements were performed using Wayne Kerr 6500B impedance analyzer.

Results and discussion

The X-ray diffraction (XRD) patterns of BFO, BNFO and BNFSO compounds are shown in Fig. 1. A trace amount of impurity phases such as $Bi_{25}FeO_{40}$ and $Bi_2Fe_4O_9$ are observed along with rhombohedral phase (which are designated as ♦ and ∗ respectively). These phases are

always formed along with the bulk BFO phase.[20] Rietveld refinement[21] is carried out to analyse the crystal structure of the compounds. From the refinement, it is evident that all compounds stabilized in rhombohedral structure with *R3c* space group. Compared to BFO, XRD pattern of BNFO compound is shifted towards the higher *2θ* side due to the substitution of smaller size Nd^{3+} (1.27 Å) ions at Bi^{3+} (1.33 Å) ion positions. On the other hand, Sc substitution in BNFO compound shifts the XRD pattern towards lower *2θ* side in BNFSO compounds. Shifting the XRD pattern towards lower *2θ* side is expected due to the substitution of larger ionic size of Sc^{3+} (0.745 Å) ion at Fe^{3+} (0.645 Å) ion positions (as shown in Fig. 1b).

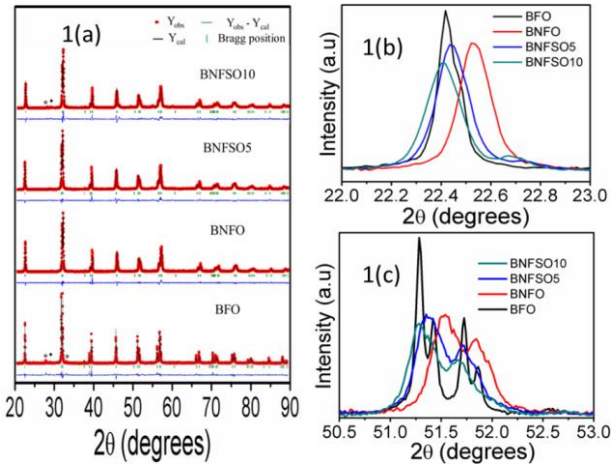

FIG. 1. (a) XRD patterns of BFO, BNFO and BNFSO compounds. The asterisks ♦ and ∗ represent impurity phases corresponding to $Bi_{25}FeO_{40}$ and $Bi_2Fe_4O_9$ respectively. (b) A typical shifting behaviour in *2θ* at around 22° & (c) XRD peak around 51° to show only the partial merging for BFO, BNFO and BNFSO compounds.

TABLE I. Lattice parameters, volume of the unit cell, bond angle and bond distance of BFO, BNFO, BNFSO5 and BNFSO10 compounds.

		BFO	BNFO	BNFSO5	BNFSO10
a (Å)		5.5794(4)	5.5756(6)	5.5846(2)	5.5915(6)
c (Å)		13.8709 (6)	13.8154(4)	13.8478(9)	13.8706(2)
Volume $(Å)^3$		373.9	372.0	374.0	375.6
Bi	*x*	0	0	0	0
	y	0	0	0	0
	z	0	0	0	0
Fe	*x*	0	0	0	0
	y	0	0	0	0
	z	0.2207	0.2239	0.2239	0.2256
O	*x*	0.4312	0.4474	0.4581	0.4786
	y	0.0018	0.0181	0.0271	0.0364

	z	0.9476	0.9522	0.9534	0.9508
Bi-O		2.310(2)	2.266(11)	2.247(11)	2.185(14)
Fe-O1		2.215(16)	2.131(8)	2.088(8)	2.087(14)
Fe-O2		1.860(17)	1.930(10)	1.972(10)	1.978(15)
Fe-O-Fe		153.2(7)	154.1(4)	155.1(4)	155.3(6)
χ^2		2.53	1.79	3.63	7.28

It is worth to mention here from the above discussion that Nd and Sc substitutions replace Bi and Fe ions respectively from their host sites and hence the corresponding changes observed in the XRD patterns. Moreover, partial merging and broadening of the doubly split peaks such as (104) & (110), (116) & (122) and (018) & (214) in vicinity of 2θ = 32º, 51º and 57º respectively are observed with the substitution of Nd and Sc ions (a typical behaviour at 2θ = 51º is shown in Fig. 1(c)). Further, no additional evolution or peaks splitting is observed which indicates the absence of any structural transition in the studied compounds. The lattice parameters *a, c* and volume of unit cell decrease in BNFO compound whereas the same increase in BNFSO compounds which is consistent with ionic size considerations. Fig. 1(b) shows the XRD peak around 22º for BFO, BNFO and BNFSO compounds. From the figure, it is revealed that the full width at half maximum (FWHM) of the peak increases from 0.100 º in BFO to 0.134º in BNFO which further increases to 0.151º in BNFSO10 compound. Increase in FWHM indicates decrease in crystallite size. Structural parameters estimated from the refinement are given in Table. I.

FE-SEM micrographs of BFO, BNFO and BNFSO compounds are shown in Fig. 2. The average grain sizes of BFO, BNFO, BNFSO5 and BNFSO10 compounds are 9 µm, 2 µm, 1.75 µm and 1.5 µm respectively which are also reflected in terms of increase in FWHM of XRD peaks. BFO has average grain size of 9 µm with a few distinct pores due to presence of oxygen vacancies formed during the synthesis at high temperatures. Larger grains are resulted due to easy diffusion of mobile oxygen vacancies. It has been observed that average grain size of BFO decreases with the substitution of Nd which is further decreased with Sc substitution.

The reduction in oxygen vacancies in the substituted compounds could be expected as the substituted elements Nd and Sc are more stable in 3+ states and have stronger bond enthalpies. The decrease in grain size could be due to lower grain growth rate which may be presumably due to the reduction in oxygen vacancies.[22] Elemental analysis studies using EDX (not shown here) are carried out and observed the atomic percentage ratio Bi (/Nd):Fe (/Sc):O is nearly close to 1:1:3 in all compounds which confirms the stoichiometry in our compounds.

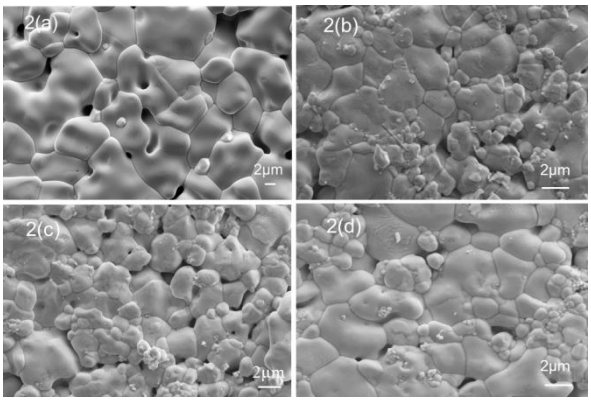

FIG. 2. FE-SEM micrographs of (a) BFO, (b) BNFO, (c) BNFSO5 and (d) BNFSO10 compounds.

The normalized Raman spectra of BFO, BNFO and BNFSO compounds are shown in Fig. 3. The natural frequency of each Raman active mode is obtained by fitting the measured spectra and deconvoluting the fitted spectra into individual Lorentzian components. For BFO, out of the thirteen possible Raman modes,[23,24] which can be summarized using the following irreducible representation: $\Gamma = 4A_1+9E$, three A_1 modes at 139, 172 and 231 cm^{-1} (can be assigned as A_1-1, A_1-2 and A_1-3 respectively) and nine E modes at 129, 261, 276, 303, 346, 369, 432, 480 and 524 cm^{-1} are observed. The A_1-1, A_1-2 and A_1-3 and E modes with frequencies less than 400 cm^{-1} are corresponding to Bi-O bonds whereas the E modes with frequencies greater than 400 cm^{-1} are corresponding to Fe-O bonds.[25] Nd substitution at A-site shows much weaker scattering intensities of A_1-2 mode (172 cm^{-1}) and E mode (261 cm^{-1}) as compared to BFO (as shown in the circles in Fig. 3). This could be due to the decline in stereochemical activity of $6s^2$ lone pair electrons of Bi which in turn affects the ferroelectric ordering.[26] The intensity of above mentioned modes increases with Sc- substitution in BNFO compounds which suggests an enhancement in the ferroelectric ordering. Also Nd substitution causes A-site disorder and hence weakens the intensity and broadens the modes (i.e., increases the FWHM of the modes as shown in the inset of Fig. 3). The broadening is more pronounced with the Sc substitution. The life times of phonons in real crystals are reduced due to the scatterings from defects, disorder, strain etc. As the FWHM is inversely proportional to life times, decrease in life times of phonons leads to increase in FWHM.[19,27] From the above discussion, it can be concluded that substitution of Nd and Sc replaces Bi and Fe respectively which is also well supported from XRD measurement.

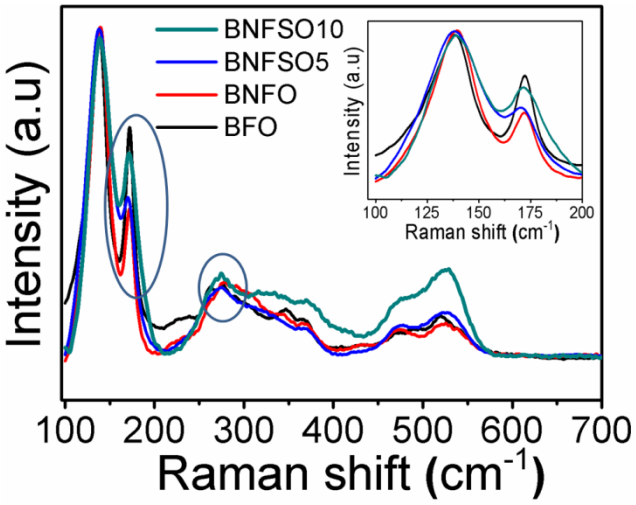

FIG. 3. Raman spectra of BFO, BNFO, BNFSO5 and BNFSO10 compounds. Inset shows the Raman spectra between 100-200 cm^{-1} for all compounds.

Fig. 4 shows the room temperature magnetization (*M*) – field (*H*) hysteresis loops of BFO, BNFO and BNFSO compounds at 300 K up to the magnetic field of 50 kÖe. BFO shows a linear field dependent narrow hysteresis loop with insignificant remnant magnetization. It has been reported that in BFO, *G*-type antiferromagnetic structure is superimposed with a spiral spin structure of incommensurate wave length of 620 Å.[20] Substitution of Nd at *A*- site distorts the crystal structure which in turn changes Fe-O distances and Fe-O-Fe bond angles and leads to enhancement in magnetization and coercive field in BNFO compound. Remnant magnetization and coercive field are further increased with the substitution of Sc in BNFO compound. The contribution of impurity phases such as Bi_2Fe4O_9 and $Bi_{25}FeO_{40}$ to magnetization is ruled out as these phases are paramagnetic at room temperature.[9,19] Remnant magnetization values are 0.6 memu/g for BFO, 30 memu/g for BNFO, 40 memu/g for BNFSO5 and 54 memu/g for BNFSO10 compound. The improved magnetic properties in terms of increase in remnant magnetization results from the suppression of SMSS with the substitution.

Since in BFO, SMSS of incommensurate wave length is 620 Å which is far larger than the lattice constants, the contribution from Fe magnetic sublattice to the magnetocrystalline anisotropy is negligible. Hence the small coercive field (235 Öe) is observed in BFO. However, the coercive field is enhanced in BNFO compound to 2.75 kÖe which is one order greater than that of BFO. Coercive field is further increased to 3.5 kÖe in BNFSO5 and to 4.7 kÖe in BNFSO10 compounds.

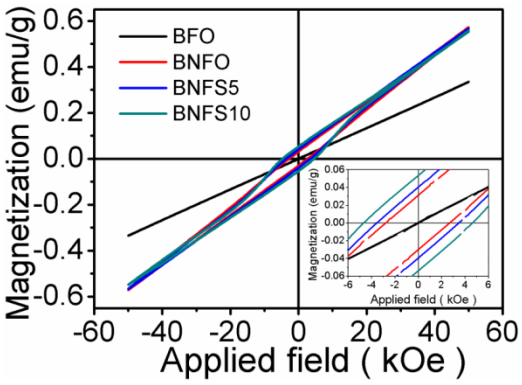

FIG. 4. Room temperature magnetization plots of BFO, BNFO and BNFSO compounds. Inset shows the enlarged view near origin.

Such high coercive fields cannot be due to pinning of magnetic domain walls alone, because the typical coercive field for such pinning is less than 0.3 kÖe.[28] High coercive fields in the substituted compounds may be due to change in magnetic anisotropy. Also, it has been reported that in case of La and Nb co-substituted BFO[29] and Pr and Zr co-substituted BFO compounds[30], increase in coercive field with the substitution is attributed to decrease in grain size which is also consistence with our findings. The non-saturating behaviour (up to applied field of 50 kÖe) with significant loop opening in substituted compounds suggests the possibility of competing antiferromagnetic and ferromagnetic interactions. It is interesting to note that the magnetization at 50 kÖe is enhanced in BNFO compound compared to that of BFO. However, substantial change in magnetization has not been observed with Sc-substitution which could be due to its diamagnetic nature.

Zero field cooled (ZFC) and field cooled (FC) magnetization measurements are carried out under a magnetic field of 1000 Öe for BFO, BNFO and BNFSO compounds as shown in Fig. 5. A small anomaly has been observed near 270 K in BFO compound, indicating spin glass-like transition similar to Singh et al,[31] which disappears in Nd and Sc co-substituted compounds. These anomalies may originate from domain wall pinning effects which are caused by random distribution of oxygen vacancies.[31] The magnetization decreases with the temperature from 300 K to 100 K suggesting the antiferromagnetic nature of the compounds up to 100 K. An abrupt increase in magnetization has been observed, especially, in the low temperature below 25 K which reveals the development of incommensurate magnetic structure in all compounds.[32] The large jump in magnetization in BNFO compound compared to that of BFO could be due to the contribution from magnetic sublattice of Nd- along with Fe sublattice. Also, the thermomagnetic irreversibility between ZFC and FC curves at 170 K increases in the BNFO compound which further increases with the Sc content. This indicates an enhancement

in weak ferromagnetism in the substituted compounds which is also confirmed from *M-H* discussion.

Fig. 6 shows the temperature variation (300 K – 750 K) of magnetization for BFO, BNFO and BNFSO compounds under the magnetic field of 1000 Öe. BFO shows antiferromagnetic to paramagnetic transition temperature (T_N) at 644 K which is well consistent the existing literature. Substitution of Nd at *A*-site affects bond distances and bond angles which in turn changes the transition temperature T_N to 633 K. Small or insignificant changes in T_N due to the substitution of rare earth elements at *A*-site has also been reported.[10,33,34] However, Sc substitution at *B*-site weakens the magnetic interaction strength and reduces T_N to 565 K in BNFSO5 and to 550 K in BNFSO10 compounds.

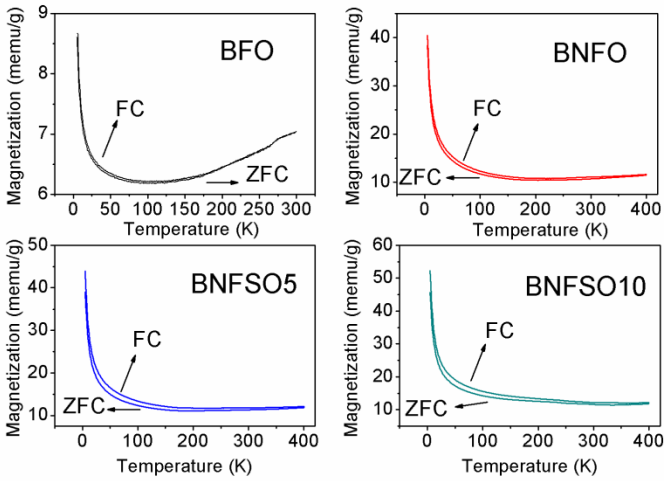

FIG. 5. ZFC and FC curves of BFO, BNFO, BNFSO5 and BNFSO10 compounds under the magnetic field of 1000 Öe.

The decrease in T_N with Sc content can also be explained using the following equation[35]

$$T_N = JZS(S+1)\cos\theta \quad (1)$$

where *J* is the magnetic exchange constant, *S* is the spin of Fe^{3+}; *Z* is the average number of linkages per Fe^{+3} ions and θ is <Fe – O – Fe> bond angle.

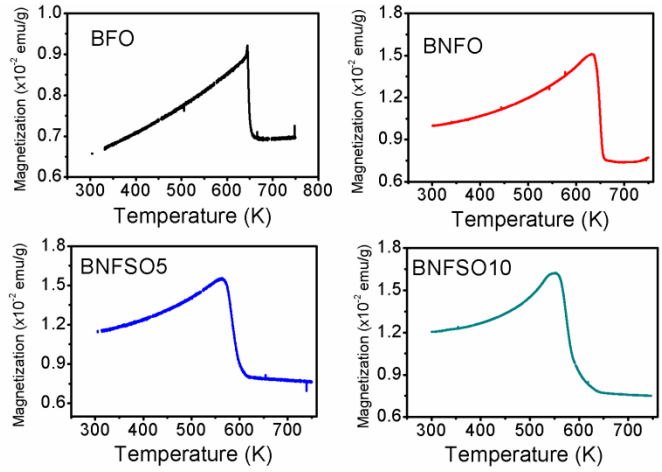

FIG. 6. Temperature dependence of magnetization for BFO, BNFO, BNFSO5 and BNFSO10 compounds under the magnetic field of 1000 Öe.

An increase in T_N is expected with the substitution of Nd and Sc due to the variation in Fe-O-Fe bond angles towards 180^o as also confirmed from Rietveld refinement analysis, however, decrease in T_N is observed here. The factor which strongly influences the reduction in T_N could be possibly due to the weakening of magnetic interactions rather than bond angle variation. Weakening in magnetic interaction is due to the presence of larger ionic size of diamagnetic Sc^{3+} ions at Fe-site. Substitution with Sc leads to existence of different types of exchange constant J such as $J_{Fe\text{-}Fe}$, $J_{Fe\text{-}Sc}$ and $J_{Sc\text{-}Sc}$ between the B-sites. The strength of $J_{Fe\text{-}Sc}$ and $J_{Sc\text{-}Sc}$ will be weaker than $J_{Fe\text{-}Fe}$ which presumably suppresses the overall J. As a result of weakening of J leads to reduction in Néel temperature.

Polarization (P) – Electric field (E) hysteresis loops of BFO, BNFO and BNFSO compounds are shown in Fig. 7. BFO shows a leaky and rounded hysteresis loop which is due to the leakage currents. The leakage currents are generated due the presence of oxygen vacancies and mixed valence states of B-site cations which are likely to exist in ABO_3 perovskite ferroelectric materials.[36] However, these vacancies are suppressed with the substitution of Nd and Sc which results well shaped and nearly saturated hysteresis polarization loops. In BFO, there exists a strong hybridization of lone pair $6s^2$ electrons of Bi^{3+} ions with $6p^0$ orbital of Bi^{3+} ion and $2p^6$ orbital of O^{2-} ion to form Bi-O covalent bonds which result the non- centrosymmetric distortions and hence ferroelectric order.[37] In the case of BNFO compound, remanent polarization (P_r = 5.4μC/cm^2) is lower than that of BFO (P_r = 9 μC/cm^2). This can be expected as Nd substitution declines the strereochemical activity and hence the reduction in remanent polarization.[38] The corresponding feature is also observed in terms of suppression of the intensity of A_1-2 (171 cm^{-1}) and E (261 cm^{-1}) modes in the normalized Raman spectra as these modes are corresponding to Bi-O modes.[26] The substitution of Sc in BNFO compound further decreases the Bi-O bond length due to the structural distortions. The shortening of the Bi-O

bonds strengthens covalent Bi-O hybridizations and causes non-centrosymmetric distortions to displace Bi^{3+} ions along $[111]_c$ direction and improves the polarizations in BNFSO compounds[39,40]. Increase in remanent polarization to 7.3 μC/cm^2 in BNFSO5 compound and to 12.5 μC/cm^2 in BNFSO10 compound is observed from the polarization measurements. The strengthening of stereochemical activity of the Bi lone pair electrons is also observed in terms of increase in the intensities of A_1-2 (171 cm^{-1}) and E (261 cm^{-1}) modes with Sc content which support the observed polarizations in BNFSO compounds. Hence, Sc substitution improves the polarizations further due to strengthening in hybridization.

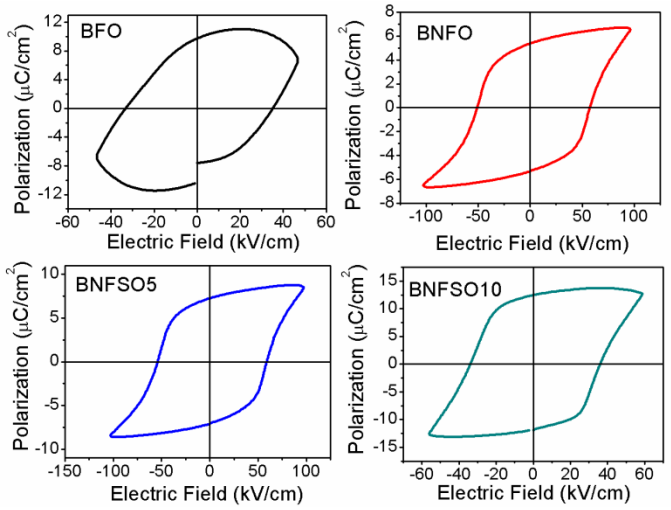

FIG. 7. *P-E* loops of BFO, BNFO, BNFSO5 and BNFSO10 compounds.

The insulating character of BFO, BNFO and BNFSO compounds can be studied using impedance spectroscopy (IS). IS spectroscopy is a non-destructive method[41] to analyse the microstructural and electrical properties of material. It provides information regarding the grain and grain boundary contributions to the electrical resistivity of BFO, BNFO and BNFSO compounds. The variation of imaginary part of complex impedance (Z'') with the real part of complex impedance (Z') (Nyquist plots) for BFO in the temperature range 30 ^{o}C to 210 ^{o}C is shown in Fig. 8(a). At low temperatures ($\leq$ 100 ^{o}C), the impedance of these compounds is very high and hence the semi-circular arcs in Nyquist plots are more inclined towards Z'' axis. Appearance of single semi-circular arc indicates electrical process are attributed to bulk (grain) in the compounds. As the temperature increases (above 100 ^{o}C), the semi-circular arc deviates towards Z' axis due to increase in the conductivity of compounds which indicates the negative temperature coefficient of resistance (NTCR) character. Further, above 150 ^{o}C, evolution of second semi-circular arc in the low frequency region is attributed to beginning of inter-granular activities (grain boundary effects) in the compounds. Hence, both grain and grain boundary effects can be separated in all compounds above 150 ^{o}C. Similar behaviour has been observed for other compounds. The impedance of resultant circuit in terms of grain resistance R_g, grain

boundary resistance R_{gb}, grain capacitance C_g and grain boundary capacitance C_{gb}, can be expressed as[42]

$$Z^* = \frac{R_g}{1+(j\omega R_g C_g)^{n_g}} + \frac{R_{gb}}{1+(j\omega R_{gb} C_{gb})^{n_{gb}}} \quad (2)$$

where n_g and n_{gb} are grain and grain boundary relaxation time distribution functions respectively. The value of n ranges from zero to unity and represents the magnitude of deviation of electrical responses from the ideal conditions. The centre of these depressed semi-circular arcs in the Nyquist plots lies below the real axis which indicates the presence of Non-Debye type relaxations. Also, the intercept of semi-circular arc on the real Z'-axis decreases due to decrease in resistivity of the compounds (NTCR character). Each semi-circular arc can be modelled in terms of electrical equivalent circuit consisting of a parallel combination of resistor R and capacitor (or constant phase element CPE) C as shown in inset of Fig. 8(b). Both grain and grain boundary resistances of BFO increase with the substitution of Nd at A- site which further increase with the Sc content at B-site. This indicates that Nd and Sc co-substitution enhances the electrical resistivity of BFO which could be due to improved barrier properties for the flow of charge carriers with the substitutions[19]. However, there is a slight decrease in grain and grain boundary resistance of BNFSO10 compound compared to grain and grain boundary resistance of BNFSO5 compound. Both R_{gb} and R_g are extracted by fitting the observed data with the equation (2) in the temperature range from 165 ^oC to 225 ^oC in all compounds. The values of R_{gb} and R_g decrease respectively from 8.4 MΩ to 1 MΩ and 0.9 MΩ to 42 kΩ for BFO, 13 MΩ to 0.50 MΩ and 2.24 MΩ to 0.12 MΩ for BNFO, 22.3 MΩ to 1.43 MΩ and 5.76 MΩ to 0.36 MΩ for BNFSO5 and 18 MΩ to 1.17 MΩ and 4.27 MΩ to 0.37 MΩ for BNFSO10 compounds in the above mentioned temperature range.

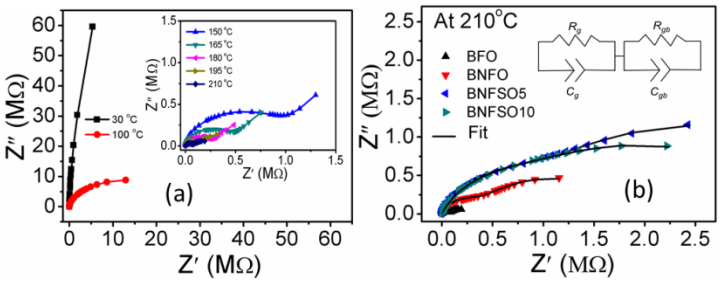

FIG. 8. (a) Nyquist plots for BFO at 30 ^oC and 100^oC. Insets shows Nyquist plots for BFO between 150 ^oC to 210^oC, (b) Nyquist plots for BFO, BNFO, BNFSO5 and BNFSO10 compounds at 210^oC.

Electric modulus formalism can also be used to study the electrical response of the material. In case of impedance formalism, intensity of relaxation peaks is corresponding to the most resistive components in the compounds whereas in modulus formalism, intensity of relaxation peaks is inversely proportional to capacitance of the compounds.

The electric modulus (M^*) is expressed as

$$M^* = M' + iM'' = i\omega C_o Z^*$$

$$= i\omega C_o (Z' - iZ'') = \omega C_o Z'' + i\omega C_o Z' \quad (3)$$

where ω is the frequency of applied electric field and C_o is the capacitance in vacuum. Frequency variation of imaginary part of electric modulus (M'') plots of BFO, BNFO, BNFSO compounds at different temperatures are shown in Fig. 9.

The value of electric modulus (M'') was calculated using the formula

$$M'' = \omega C_o Z' \quad (4)$$

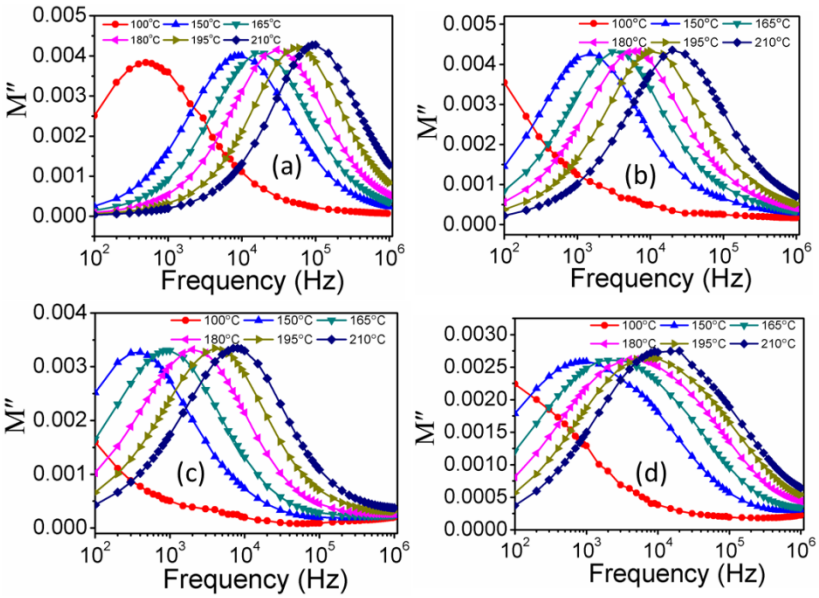

FIG. 9. Frequency variation of imaginary part of complex electric modulus (M'') plots for (a) BFO, (b) BNFO, (c) BNFSO5 and (d) BNFSO10 compounds.

At low frequency region, M'' shows very small values due to the high value of capacitance and exhibits a peak in the high frequency region. These peaks are not observed in the frequency dependent dielectric data (not shown here), but are clearly seen in the modulus data. These peaks are generally characterized by significant broadening and shifting of peak position towards high frequency region with the rise of temperature. Broadening in the peak indicates the presence of distribution of relaxation times and hence the relaxation is of non-Debye type. The shifting of peak position indicates the relaxation process is thermally activated.

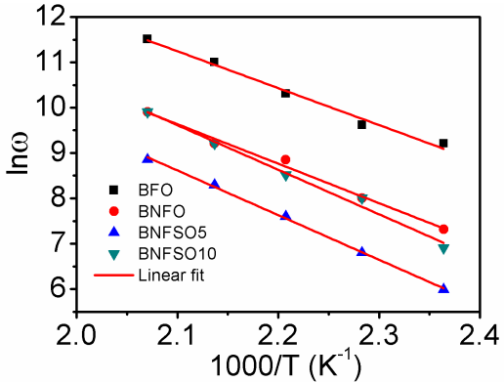

FIG. 10. Arrhenius plot of lnω versus 1000/T for (a) BFO, (b) BNFO, (c) BNFSO5 and (d) BNFSO10 compounds.

The frequency region below the peak value of M'' (M''_{max}) indicates the range of frequencies for the charge carriers to perform long range hopping from one site to another site where as frequencies above M''_{max}, charge carriers perform short range hopping and the charged particles are confined to their potential wells and execute only localized motions. The frequency (ω_{max}) corresponding to the M''_{max} gives the most probable relaxation time (τ_{max}) for the charge carriers and follows the Arrhenius law

$$\omega_{max} = \omega_o e^{-E/kT} \quad (5)$$

where ω_o is the pre exponential factor and E is the activation energy. The activation energies are calculated from the slope of the plot (shown in Fig. 10) drawn between ln(ω_{max}) and 1000/T. The obtained activation energies for BFO, BNFO, BNFSO5 and BNFSO10 compounds are 0.69±0.04, 0.75±0.04, 0.85±0.02, 0.85±0.05 eV respectively. The typical activation energy values associated for singly ionised oxygen vacancies are in the range 0.3 – 0.5 eV whereas for doubly ionised oxygen vacancies, activation energies are in the range 0.6 – 1.2 eV for a perovskite based oxide materials.[43] The observed activation energies indicate that doubly ionised oxygen vacancies are responsible for the relaxation process. Overall, impedance analysis confirms an improvement in insulating character in Sc-substituted compounds which is also consistent with the observation of near to saturation *P-E* loops as well as improved ferroelectric ordering.

Conclusions

Polycrystalline $BiFeO_3$ and $Bi_{0.9}Nd_{0.1}Fe_{1-x}Sc_xO_3$ (x = 0, 0.05 and 0.10) compounds were prepared using solid state reaction technique. Room temperature XRD and Raman studies revealed that compounds crystallized in rhombohedral structure with *R3c* space group. Induced weak ferromagnetism in the substituted compounds was mainly attributed to suppression of modulated spin structure. Reduced Néel temperature in BNFSO5 and BNSFO10 compounds could be due to weakening of magnetic exchange interactions due to the presence of larger diamagnetic Sc^{3+} ions in place of Fe^{3+} ions. Improved ferroelectric properties in the substituted compounds were attributed to the strengthening of covalent hybridization between Bi and O ions and reduction in oxygen vacancies. Improved insulating character in terms of improved grain and grain boundary resistances were observed in the substituted compounds due to structural distortions. Doubly ionised oxygen vacancies were responsible for the dielectric relaxation process. Reduced Néel temperature down towards room temperature and enhancement of magnetic and electrical properties demonstrate its potential use in device applications.

Acknowledgements

Authors are grateful to the Department of Science and Technology (DST), Government of India for their financial support under Fast Track scheme (SR/FTP/PS–065/2011) to carry out this work.

References

[1] K. M. Song, Y. A. Park, K. D. Lee, B. K. Yun, M. H. Jung, J. Cho, J. H. Jung, and N. Hur, Phys. Rev. B **83**, 012404 (2011).

[2] W. Eerenstein, N. D. Mathur, and J. F. Scott, Nature **442**, 759 (2006).

[3] J. B. Neaton, C. Ederer, U. V. Waghmare, N. A. Spaldin, K. M. Rabe, Phys. Rev. B **71,** 014113 (2005).

[4] J. R. Teague, R. Gerson, W. J. James, Solid State Commun. **8,** 1073 (1970).

[5] J. M. Moreau, C. Michel, R. Gerson, W. J. James, J. Phys. Chem. Solids **32**, 1315 (1971).

[6] C. Michel, J.-M. Moreau, G. D. Achenbach, R. Gerson, and W. J. James, Solid State Commun. **7**, 701 (1969).

[7] J. L Xu, Dan Xie, Cong Yin, T. T. Feng, X. O. Zhang, G. Li, H. Zhao, Y. F. Zhao, Shuo Ma, T. L. Ren, Y. J. Guan, X. S. Gao, and Y. G. Zhao, J. Appl. Phys. **114**, 154103 (2013).

[8] J. K. Kim, S. S. Kim, W. J. Kim, A. S. Bhalla, and R. Guo, Appl. Phys. Lett. **88**, 132901 (2006).

[9] T. D. Rao, T. Karthik, and S. Asthana, J. Rare Earths **31**(4), 370 (2013).

[10] T. D. Rao, T. Karthik, A. Srinivas, and S. Asthana, Solid State Commun. **152**, 2071 (2012).

[11] W. Weia, H. C. Xuan, L. Wang, Y. Zhang, K. Shen, D. H. Wang, T. Qiu, Q. Xu, Physica B **407,** 2243 (2012).

[12] T. D. Rao, A. Kumari, M. K. Niranjan, S. Asthana, Physica B **448**, 267 (2014).

[13] S. Yasui, H. Uchida, H. Nakai, K. Nishida, H. Funakubo, S. Koda, Appl. Phys. Lett. **91,** 022906 (2007).

[14] Y. F. Cui, Y. G. Zhao, L. B. Luo, J. J. Yang, H. Chang, M. H. Zhu, D. Xie, T. L. Ren, Appl. Phys. Lett. **97**, 222904 (2010).

[15] J. S. Park, Y. J. Yoo, J. S. Hwang, J.-H. Kang, B. W. Lee, and Y. P. Lee, J. Appl. Phys. **115**, 013904 (2014).

[16] M. A. Basith, O. Kurni, M. S. Alam, B. L. Sinha, and Bashir Ahmmad, J. Appl. Phys. **115**, 024102 (2014).

[17] Reetu, A. Agarwal, S. Sanghi, Ashima, Neetu Ahlawat, J. Appl. Phys. **113**, 023908 (2013).

[18] J. A. Kerr, C R C Handbook of Chemistry and Physics, 81st ed., CRC Press, Boca Raton, Florida, USA, 2000.

[19] T. D. Rao, R. Ranjith, and S. Asthana, J. Appl. Phys. **115,** 124110 (2014).

[20] I. Sosnowska, T. Peterlin-Neumaier, E. Steichele, Phys C **15**, 4835 (1982).

[21] J. Rodrigues-Carvajal, FULLPROF. A Rietveld Refinement and Pattern Matching Analysis Program (Laboratoire Leon Brillouin, CEA-CNRS, France, 2000).

[22] C. F. Chung, J.P Lin, J. M. Wu, Appl. Phys. Lett. **88**, 242909 (2006).

[23] R. Haumont, J. Kreisel, P. Bouvier, and F. Hippert, Phys. Rev. B **73**, 132101 (2006).

[24] H. Fukumura, H. Harima, K. Kisoda, M. Tamada, Y. Noguchi, and M. Miyayama, J. Magn. Magn. Mater. **310**, 367 (2007).

[25] M. K. Singh, S. Ryu, and H. M. Jang, Phys. Rev. B **72**, 132101 (2005).

[26] G. L. Yuan, Siu Wing Or, and Helen Lai Wa Chan, J. Appl. Phys. **101**, 064101 (2007).

[27] Z. Quan, W. Liu, H. Hu, S. Xu, B. Sebo, G. Fang, M. Li, and X. Z. Zhao, J. Appl. Phys. **104**, 084106 (2008).

[28] E. C. Stoner, Rep. Prog. Phys. **13**, 83 (1950).

[29] L. Zhai, Y.G. Shi, S. L. Tang, L. Y. Lv, Y. W. Du, J. Phys. D: Appl. Phys. **42**, 165004 (2009).

[30] P. C. Sati, M. Arora, S. Chauhan, S. Chhoker, M. Kumar, J. Appl. Phys. **112**, 094102 (2012).

[31] M. K. Singh, W. Prellier, M. P. Singh, R. S. Katiyar, and J. F. Scott, Phys.Rev. B **77**, 144403 (2008).

[32] Z. P. Chen, C. Wang, T. Li, J. H. Hao, J. C. Zhang, J Supercond Nov Magn. **23,** 527 (2010).

[33] D. Kothari, V. Raghavendra Reddy, A. Gupta, V. Sathe, A. Banerjee, S. M. Gupta, A. M. Awasthi, Appl. Phys. Lett. **91,** 202505 (2007).

[34] S. Saxin, Ch. S. Knee, J. solid state chem, **184**, 1576 (2011).

[35] M. A. Ahmed, S. I. El-Dek, Mater. Lett. **60**, 1437 (2006).

[36] O. D. Jayakumar, S. N. Achary, K. G. Girija, A. K. Tyagi, C. Sudakar, G. Lawes, R. Naik, J. Nisar, X. Peng, R. Ahuja, Appl. Phys. Lett. **96,** 032903 (2010).

[37] G. L. Yuan, Siu Wing Or, J. M. Liu, Z. G. Liu, Appl. Phys. Lett. **89**, 052905 (2006).

[38] A. Kumar, D. Varshney, Ceramics International **38,** 3935 (2012).

[39] K. Fujii, H. Kato, K. Omoto, M. Yashima, J. Chen and X. R. Xing, Phys. Chem. Chem. Phys. **15**, 6779 (2013).

[40] J.-B. Li, G.H. Rao, Y. Xiao, J.K. Liang, J. Luo, G.Y. Liu, J.R. Chen, Acta Materialia **58,** 3701 (2010).

[41] J. R. Macdonald, Impedance Spectroscopy: Emphasizing Solid-State Material and Systems, Wiley, New York, 1987, ch. 2 and ch.4.

[42] A. Singh, R. Chatterjee, S. K. Mishra, P. S. R. Krishna, and S. L. Chaplot, J. Appl. Phys. **111**, 014113 (2012).

[43] S. Sarangi, T. Badapanda, B. Behera, S. Anwar, Mater. Electron. **24**, 4033 (2013).